Published in final edited form as:
Magn Reson Imaging. 2011 April ; 29(3): 315–323. doi:10.1016/j.mri.2010.10.003.

Earlier Detection of Tumor Treatment Response Using Magnetic Resonance Diffusion Imaging with Oscillating Gradients

Daniel C. Colvin[1,2], **Mary E. Loveless**[1,4], **Mark D. Does**[1,3,4], **Zou Yue**[1], **Thomas E. Yankeelov**[1,3,4,5,7], and **John C. Gore**[1,2,3,4,6,7]

[1]Institute of Imaging Science, Vanderbilt University, Nashville, TN, USA

[2]Department of Physics and Astronomy, Vanderbilt University, Nashville, TN, USA

[3]Department of Radiology and Radiological Sciences, Vanderbilt University, Nashville, TN, USA

[4]Department of Biomedical Engineering, Vanderbilt University, Nashville, TN, USA

[5]Department of Cancer Biology, Vanderbilt University, Nashville, TN, USA

[6]Department of Molecular Physiology and Biophysics, Vanderbilt University, Nashville, TN, USA

[7]Vanderbilt Ingram Cancer Center, Vanderbilt University, Nashville, TN, USA

Abstract

An improved method for detecting early changes in tumors in response to treatment, based on a modification of diffusion-weighted magnetic resonance imaging, has been demonstrated in an animal model. Early detection of therapeutic response in tumors is important both clinically and in pre-clinical assessments of novel treatments. Non-invasive imaging methods that can detect and assess tumor response early in the course of treatment, and before frank changes in tumor morphology are evident, are of considerable interest as potential biomarkers of treatment efficacy. Diffusion-weighted magnetic resonance imaging is sensitive to changes in water diffusion rates in tissues that result from structural variations in the local cellular environment, but conventional methods mainly reflect changes in tissue cellularity and do not convey information specific to micro-structural variations at sub-cellular scales. We implemented a modified imaging technique using oscillating gradients of the magnetic field for evaluating water diffusion rates over very short spatial scales that are more specific for detecting changes in intracellular structure that may precede changes in cellularity. Results from a study of orthotopic 9L gliomas in rat brains indicate that this method can detect changes as early as 24 hours following treatment with 1,3-bis(2-chloroethyl)-1-nitrosourea (BCNU), when conventional approaches do not find significant effects. These studies suggest that diffusion imaging using oscillating gradients may be used to obtain an earlier indication of treatment efficacy than previous magnetic resonance imaging methods.

Keywords

Magnetic resonance imaging; diffusion imaging; therapeutic response; tumor microenvironment; noninvasive biomarker

Address for correspondence: Dr. John C. Gore, 1161 21st Ave South, Medical Center North AAA-3107, Nashville, TN 37232-2310, john.gore@vanderbilt.edu.

1. Introduction

The early detection of the response of tumors to therapy is important both clinically and in pre-clinical assessments of novel treatments. In clinical practice, the early recognition of failure to respond to a specific treatment may allow alternative regimens to be explored and avoid unnecessary patient exposure to harmful side effects. In the evaluation of novel pharmacological therapies in pre-clinical studies, sensitive assessments of changes in tumor state, and of the time course of tumor response, are important indices of therapeutic efficacy that may affect decisions in drug development. Non-invasive imaging methods that can detect and assess tumor response early in the course of treatment, and before frank changes in tumor morphology are evident, are therefore of considerable interest as potential biomarkers of treatment efficacy. To this end, a variety of approaches using magnetic resonance imaging (MRI) have been explored, including dynamic contrast enhanced MRI (DCE-MRI) [1–4], which has proven especially useful for assessing tumor vascular properties and angiogenesis, and diffusion weighted MRI (DW-MRI) [5–8], which has been shown to be able to monitor changes in tissue cellularity. These specialized methods complement the more standard uses of MRI as a valuable tool in cancer diagnosis and for measuring tumor size in clinical trials.

Several clinical and animal studies have confirmed the ability of conventional DW-MRI to report on changes in tumors at some time after treatment [9–14]. DW-MRI relies on the phenomenon that water molecules in tissues constantly undergo random Brownian motion and diffuse from place to place at a rate that is temperature dependent. In MRI, in the presence of applied gradients of the magnetic field, this spatial migration gives rise to small changes (decreases) in the acquired MRI signals, which thus provides the basis of the contrast depicted in DW-MRI. The experimentally measured or apparent rate of self-diffusion of tissue water is lower in organized tissues than in free solution because various structures restrict or hinder the free movement of water. For example, cell membranes and intracellular organelles may confine and redirect the paths followed by water molecules diffusing through biological tissue, so DW-MRI methods indirectly provide information about the density of restrictive structures in the local cellular environment. The apparent diffusion coefficient (ADC) thus provides information about tissue microstructure and composition, and is reduced from the intrinsic diffusion coefficient D_0 of free water to a degree that is dependent upon the density and spacing of these restricting structures.

Cancerous tissues often show significantly different ADC values from healthy tissues, providing motivation for the use of DW-MRI techniques to study tumor proliferation and response to therapy. As tumor cells proliferate, the ADC of water within the tumor often decreases as cell density rises, whereas after treatment the ADC often increases, presumably because of decreases in cell density consequent to apoptosis and cell death, with concomitant disruption of cell membranes. Such changes occur only after a critical time has elapsed and thus are not ideal for assessing early responses. While this increase in ADC following treatment can often be linked to a decrease in cellularity [9–14], the aggressive nature of malignant tumors necessitates a more sensitive approach for evaluating the response of cancer cells prior to such macroscopic changes. In particular, it would be of considerable interest to possess non-invasive imaging biomarkers of treatment response that are specifically sensitive to variations in intracellular structure that likely occur earlier in time.

Conventional MRI methods used to measure diffusion actually reflect the integrated effects of a variety of structural features including those arising at a relatively large spatial scale, on the order of a cell diameter, such as cell membranes. Many other factors may influence the

free movement of water, including changes in intracellular organization and the presence of smaller scale hindrances, but their effects are indistinguishable in the presence of restrictions occurring over larger dimensions when the measurement is made with conventional methods. This lack of specificity arises from the fact that practical diffusion measurements incorporate a particular chosen time scale, during which water diffusion effects over multiple distance scales are averaged. When this time is long, as in conventional DW-MRI, these are dominated by larger scale structures in tissues. We have therefore implemented an oscillating gradient spin-echo (OGSE) MRI technique capable of detecting restrictions to diffusion displacements over much smaller and specific spatial scales, which can be "tuned" by choice. These may be selected to be much less than the diameter of a single cell, which results in a greater sensitivity specifically to the contributions of structures at sub-cellular scale to the measured ADC. In a previous report we illustrated the use of this method for providing greater image contrast and detecting increased structural heterogeneity in an intracranial tumor model in rats *in vivo* [15]. The current study extends these techniques to the evaluation of tumor state following treatment with the commonly used chemotherapeutic drug 1,3-bis(2-chloroethyl)-1-nitrosourea (BCNU or Carmustine), in order to evaluate whether they show increased sensitivity for detecting early treatment responses.

Malignant gliomas are the most prevalent and lethal primary tumors of the central nervous system. Despite significant advances in surgical intervention and radio- and chemotherapeutic treatments, median survival times following diagnosis of this disease are reported to be less than one year [16–17]. We chose to test the sensitivity of DW-MRI for detecting treatment effects in vivo in an animal model, a 9L glioblastoma tumor in rats. The effects of BCNU on tumor ADC values after treatment were measured using our modified and conventional DW-MRI techniques, and the potential for the new approach to serve as an earlier indicator of treatment response is demonstrated.

2. Materials and Methods

2.1 Animal Model

All procedures in this study were approved by Vanderbilt University's Institutional Animal Care and Usage Committee. Eighteen male Fischer 344 rats, weighing approximately 250g, were immobilized and anesthetized with a 2%/98% isoflurane/oxygen mixture and inoculated intracranially with ~10^5 9L glioblastoma cells (ATCC 9L/lacZ, CRL-2200). The 9L cell line was authenticated by the distributor (ATCC, Manassas, VA, USA) through detection of the β-galactosidase enzyme, and maintained within our laboratory for fewer than six months before collection for inoculation. Eleven (N_{TX} = 11) rats were treated with BCNU as described below, and seven (N_{CON} = 7) were used as untreated, tumor-bearing controls. The tumors were allowed to develop untreated for 11–12 days. All animals were imaged immediately before and 24 hours after treatment. Five animals (3 treated, 2 controls), were sacrificed following the 24 hour post-treatment imaging session in order to obtain histology for this time point. All surviving animals (N_{TX} = 8 and N_{CON} = 5) were also imaged 72 hours post-treatment, after which they were euthanized and tissues examined histologically as described below.

2.2 Treatment protocol

BCNU, also known as Carmustine (1,3-bis(2-chloroethyl)-1-nitrosourea) is an antineoplastic chemotherapy drug used primarily in the treatment of brain tumors [18–22], as well as melanoma, Hodgkin's disease, and lung cancer (23–27). BCNU is a cell cycle-nonspecific alkylating agent which cross-links nuclear DNA, inhibiting DNA synthesis and promoting cell death.

Treatment solutions were prepared by dissolving a 13.3 mg/kg powdered dose in ethanol, and diluting with saline to achieve a 10/90% ethanol/saline solution totaling approximately 1 mL in total volume. The dose of 13.3 mg/kg has been shown in previous studies to produce an approximate 0.2 log cell kill in 9L tumors, and is equal to a 10% lethal dose [28–31]. Control animals received vehicle only (1mL of 10/90% ethanol/saline). The treatment protocol consisted of a single intra-peritoneal injection of BCNU (or sham) immediately following the initial imaging session (Day 0).

2.3 In vivo imaging

Approximately eleven days following tumor inoculation, MR images were obtained using a Varian 4.7T Inova imaging system (Palo Alto, CA, USA). Animals were anesthetized with a 2%/98% isoflurane/oxygen mixture, and kept at a constant body temperature of 37° C with heated air flow. A rigid bite-bar and head restraint were used to ensure proper positioning, as well as to reduce motion-induced artifacts in the image data.

Images were acquired using a quadrature 63mm inner diameter radiofrequency coil. On the initial day of imaging for each animal, a multi-slice, T2-weighted fast spin echo scan with 4 echoes (TR= 2000, 16ms echo spacing, 256×128 matrix, 48×32mm^2 FOV, 1mm slice thickness) was acquired in the coronal plane for locating the tumor region. A subsequent 2mm single axial slice (same timing parameters, but FOV = 32×32mm^2) through the central portion of the tumor was then acquired for anatomical clarification of the tumor boundary in subsequent region-of-interest (ROI) analysis. The same slice was then imaged using our oscillating gradient spin-echo technique. For this, the pulsed linear field gradients used to induce diffusion-dependent signal losses in conventional DW-MRI are simply replaced with cosinusoidally oscillating gradients of a well defined frequency, applied in bursts of duration 33.33 ms, as described previously [15]. We chose oscillation frequencies of 120 Hz and 240 Hz which are readily achievable using the standard Varian gradient coils. Diffusion-weighted scans were collected with b-values of 0 and 400 s/mm^2 with TR/TE = 2300/75.4ms, 64×64 matrix size, 2 mm slice thickness, 32×32mm^2 FOV. and NEX = 10. Following the OGSE imaging, conventional pulsed gradient spin echo (PGSE) diffusion-weighted images were also obtained, with the same b-values, with gradient duration $\delta = 3$ ms and diffusion interval $\Delta = 30$ ms. An additional PGSE scan at the non-zero b-value was also obtained with reversed gradient polarity, and averaged with the first to eliminate the presence of gradient cross-terms in the ADC measurements [32]. These cross-terms are absent in our version of the OGSE technique. In all cases, diffusion gradients were placed along all three imaging coordinate axes simultaneously to maximize the diffusion weighting with the available gradient amplitudes.

Consistent selection of the single slice imaging planes from pre- to post-treatment time points was achieved using a mutual information based rigid registration algorithm. On each day of scanning, a 3D gradient echo image dataset (TR/TE = 25/2.2 ms, FOV = 48 × 32 × 32 mm^3, matrix = 128 × 96 × 96, NEX = 8) encompassing the whole brain was collected. On Days 1 and 3 following treatment, these 3D images were co-registered to the initial 3D image collected on Day 0 in order to derive the translation and rotation matrices of the animal's position with respect to it's pre-treatment position in the laboratory reference frame. These translations and rotations were then applied to the coordinates of the single pre-treatment slice in order to obtain the same section during post-treatment imaging. Given the rigid construction of the imaging cradle and animal bite-bar, the translation and rotation of each rat brain between imaging sessions was minimal. The single slice images for each animal at all time points were then co-registered (via mutual information) following data reconstruction as well. From previous studies, the accuracy of coregistration is of the order of 0.5 millimeters.

2.4 Perfusion fixation

Immediately following the imaging sessions at 24 or 72 hours post-treatment, several rats remained anesthetized and were anti-coagulated with 80 mg/kg pentobarbital i.p. mixed with 0.01 ml/100 g heparin. A surgical incision was then performed to allow a blunt 16 gauge perfusion needle to be inserted into the left cardiac ventricle toward the left ventricular outflow tract, and just into the aorta. A saline wash solution was then perfused, with the right atrial appendage cut immediately to allow the rapid outflow of blood and wash solution. At this time, the perfusate was switched to 10% formalin. Fixation began at a high flow rate (50 cc/min) for 2–5 minutes, then decreased to a slower rate (20 cc/min) for several minutes. The whole brain tissue was then dissected and placed in fixative solution. Approximately 48 hours later, the fixative was removed and the brain was placed in 70% ethanol until sectioned.

2.5 Histological sectioning, staining, and analysis

In order to obtain preliminary indications of histological changes within the tissues, seven fixed rat brain samples treated with BCNU (five sacrificed 72 hours after treatment, two sacrificed 24 hours after treatment), as well as five fixed brain samples from controls (three from the 72 hour group, two from the 24 hour group) were prepared by the Vanderbilt University Immunohistochemistry Core for sectioning and staining. Each brain was embedded in paraffin wax and sectioned in 10 micron thick axial slices across the whole brain and through the central portion of the tumor congruent with the imaging slice. Fifteen serial slices were obtained, treated with one of three stains (H&E, Ki-67, or Casp-3) in an interleaved manner, and then mounted on glass slides for a total of five slides for each stain.

Digital images of each stained histology slide were then collected with a Zeiss Mirax Scan Digital microscope slide scanner at 40× magnification, and exported using Mirax Viewer software (Mirax, Budapest, Hungary). ImageJ software [33] was used to segment positively stained cells in the Ki-67 and Casp-3 slides by the k-means clustering algorithm [34–36], and the area fraction of positively stained cells was recorded. The Ki-67 antigen is expressed during all phases of mitosis except the resting phase (G0), and thus serves as a useful marker of cell proliferation. Casp-3 detects caspases within cells, and thus is a marker of apoptosis. A comparison of the number of positively stained Ki-67 cells and Casp-3 cells between treated and untreated animals also provides information about the antineoplastic, apoptotic, and necrotic effects of the BCNU treatment.

In addition, hemotoxylin and eosin (H&E) stains were also obtained to depict gross cellular morphology and to demonstrate boundaries the boundaries between intra-nuclear, intra-cellular, and extracellular space. We were therefore able to use the ImageJ software to calculate the relative area fractions of each space by counting the number of pixels whose data values fell into one of three data clusters using the k-means algorithm. The results of this analysis are outlined in the Results section and Table 1 below.

2.6 Calculation of ADC maps

ADC values were obtained by fitting the attenuated signal in each voxel, *S*, to the equation:

$$S = S_0 e^{-b.ADC} \quad (1)$$

where S_0 is the signal in the absence of diffusion weighting, and *b* represents the amount of diffusion-weighting imparted to the sample [37]. This magnitude of the *b*-value depends on the precise nature (the amplitude, duration and time-dependence) of the applied gradients as described previously [38]. The b-values were calculated for the different gradient waveforms, and gradient amplitudes were adjusted to match the diffusion weighting

between different acquisitions as described previously [15, 38]. The effective diffusion time for OGSE methods depends on the oscillation frequency. For diffusion in an unbounded medium (no restrictions), at a frequency of 240 Hz, the effective diffusion time ≈ 1 millisecond, 30 times smaller than for the PGSE measurements. (For a more complete description of these calculations, see reference 38). Note that the effective diffusion time in OGSE depends on the oscillation period only, and is no longer determined by the time between gradient pulses. The signal to noise ratios in both PGSE and OGSE images were very similar.

All data were analyzed using Matlab 2009a (The Mathworks, Natick, MA, USA). Whole tumor regions of interest were drawn and segmented with reference to high-resolution T_2-weighted scans, and may have included additional voxels on Day 1 and Day 3 following treatment (or sham) due to increased tumor volume at these imaging time points. Statistical analyses (t-tests) comparing the ADC measurements were used to determine the significance of the results reported below.

3. Results

Fig. 1 shows representative ADC maps obtained with OGSE and PGSE methods for one animal treated with BCNU. These images demonstrate the higher values and broader range of ADC values obtained with OGSE methods and the greater spatial heterogeneity found within the tumor, especially following chemotherapeutic treatment. While the conventional (PGSE) images show a slight increase in ADC following treatment, the OGSE techniques show larger changes at early time points (see below). This is consistent with our prediction that OGSE methods may detect changes in tissue structure occurring on an intracellular scale, before gross changes in cell density.

Histograms of ADC values within a whole tumor region of interest (for the animal shown in Fig. 1) are plotted in Fig. 2. These plots reveal the range of ADCs measured with each technique, as well as the increase in mean ADC as a function of treatment. Note that the maximum ADC values measured by PGSE are still much lower than the value for free water, suggesting all the water is hindered when the diffusion time is long (30 milliseconds), whereas the OGSE data at 240 Hz after treatment show a number of voxels have ADC values approaching that of free water, suggesting a loss of structures that hinder diffusion at this shorter time scale. These results are further illustrated in Fig. 3, which shows the relationship between pre- vs post-treatment ADCs for all voxels within the tumor. There is an increase in ADC measured with both techniques 24 hours following treatment. The range of ADC values broadens after 72 hours, indicating a greater range in the sizes of restrictive structures present in the cellular environment.

Fig. 4 shows the mean ADC across all animals at all three imaging time points, using OGSE and PGSE methods. Note that ADC values shown here are the mean values across the entire tumor, and greater differences in OGSE ADCs pre- and post-treatment are present in many voxels (as indicated in Fig. 1). The control group showed no significant changes in ADC at all imaging time points, for all methods. The ADC of the treated animals, however, clearly increases with time after treatment. After 24 hours, the ADC increased from 1.16 ± 0.10 μm^2/ms to 1.19 ± 0.12 μm^2/ms at 120 Hz, an approximately 2.5% change, while it increased by approximately 4% at 240 Hz, from 1.27 ± 0.11 μm^2/ms to 1.33 ± 0.12 μm^2/ms. At the same time point, there was an approximate 1.5% increase with PGSE methods, from 0.855 ± 0.12 μm^2/ms to 0.869 ± 0.13 μm^2/ms. At 24 hours, paired student t-tests showed the changes measured by OGSE techniques to be significant at the $\alpha = 0.05$ level ($p = 0.04$ and $p = 0.024$, at 120 Hz and 240 Hz respectively), but not significant for PGSE ($p = 0.13$). After 72 hours, both imaging methods revealed statistically significant increases in ADC, increasing

by approximately 18% (120 Hz) and 20% (240 Hz) from their pre-treatment values, as measured with OGSE, and by approximately 16% with PGSE. Statistical measures of significance gave p-values, at 72 hours, of $p = 0.009$ (120 Hz), $p = 0.003$ (240 Hz), and $p = 0.018$ (PGSE). Statistical analyses of the control animals gave p-values greater than $p > 0.05$ in all cases.

As previously described, a k-means clustering algorithm (ImageJ) was used for segmentation of whole tumor regions of interest from histological image data. Mean area fractions of positively stained cells in Ki-67 and Casp-3 marked slides were recorded for both treated and control animals. Area fractions of hemotoxylin-stained, eosin-stained, and unstained portions of the H&E slides, for both groups, were also recorded. An example is shown in Fig. 5.

The relatively small number of samples available in this study did not permit strong conclusions to be made about possible correlations between histological and imaging data, or to reliably detect differences in the histological measurements between groups and time points. We attempted to look for trends and differences with statistical assessments using unpaired student t-tests at a significance level of $\alpha = 0.05$. The measurements of area fractions and their comparisons are summarized in Table 1. For example, we could not detect significant differences in the area fractions of positively stained Casp-3 (apoptotic) cells between groups either at twenty-four or seventy-two hours after treatment. Similarly, we could not detect differences in the area fractions of positively stained Ki-67 (proliferating) cells 24 hours after treatment. Seventy-two hours after treatment, however, the percentage for the treated group fell, while the control group increased, consistent with the expected antineoplastic effects of BCNU on the number of proliferating cells in treated animals, while the untreated tumors continued to grow. At 24 hours, we were also unable to detect significant differences in the extracellular area fraction, suggesting the cellularities of the treated and control groups were not different at that time.

4. Discussion

Our measurements and analyses reveal that OGSE techniques at moderately high frequencies may provide an earlier and more sensitive indicator of tumor treatment response than conventional, pulsed-gradient (PGSE) methods. The broader range of ADC values obtained with OGSE techniques provide greater contrast in corresponding ADC maps, and reveal details of tissue microstructure obscured by conventional means. While PGSE methods have been shown to be sensitive to changes in tumor cellularity resulting from treatment response, their inability to measure diffusion processes on an intracellular scale renders these methods less sensitive to microstructural variations that may precede changes in cellularity. Therefore, the results obtained with OGSE methods may be of particular interest for assessing the efficacy of therapeutic agents noninvasively, prior to changes in tumor size.

The difference in the mean ADCs measured by PGSE and OGSE methods implies that there is a significant difference in the number of restrictions encountered by water molecules during these two types of experiments. The PGSE studies used a relatively long diffusion time (30 ms), during which an unrestricted water molecule would travel approximately 12 microns, a distance comparable to a cell diameter. The ADC of water measured with PGSE methods in this study was much lower than that of free water (~2.5 $\mu m^2/ms$ at body temperature), indicating that restrictions occurred on scales smaller than 12 microns. However, given that an unrestricted water molecule would move only approximately 2 microns during the effective diffusion time of the 240 Hz OGSE measurement (1 ms), the much higher ADC in this case indicates much less (but still significant) restriction at the 2

micron spatial scale. It will therefore be of interest to measure biological samples at different and shorter effective diffusion times in order to glean information about the range of restrictions occurring in the intracellular environment.

These studies have shown that OGSE methods are capable of revealing significant differences in tumor ADC only 24 hours after treatment with an anti-neoplastic chemotherapeutic agent, whereas PGSE techniques showed no such effect. The quantitative histological analysis at 24 hours, although based on only a small number of samples, suggests that the fraction of proliferating and/or apoptic cells as well as the total fraction of extracellular space were not significantly different in treated vs control tumors. We postulate that the significant differences in ADC measured by OGSE techniques are not caused by changes in cellularity, but may arise from variations in intracellular structure that occur earlier. While PGSE measurements were capable of revealing such differences after 72 hours, the effects were smaller and these methods were incapable of resolving differences at the earlier time point.

Recent evidence suggests that nuclear volume may play a significant role in cancer diagnosis, as well as prognosis following treatment [39–41]. Xu, et al, [42] recently reported the results of numerical simulations of the effects that differences in the nuclear/cytoplasmic volume ratio of cells would have on ADC measurements. This study reported that OGSE methods might reveal differences in ADC as large as 15% at oscillation frequencies up to 1 kHz, for two tissues with the same cell density but nuclear/cytoplasmic volume ratios of 6.2% and 22%, while PGSE showed little difference over a broad range of diffusion times (< 3.6%). We report here an approximate 4% increase in ADC using OGSE methods 24 hours following treatment, compared to approximately 1.5% with PGSE. While these differences are smaller than those reported by Xu. et al., our experiments were performed at much lower oscillation frequencies (120 Hz and 240 Hz), with smaller differences in the mean nuclear/cytoplasmic ratios between groups. Given the relatively small number of samples studied by histology, we were unable to detect significant differences in extracellular space between treated and control animals after 24 hours, but those measurements suggest there were little to no differences in cellularity, consistent with the conjecture that OGSE methods may be capable of detecting changes in ADC that result from other effects, such as changes in intracellular structure or nuclear volume.

While previous studies implementing OGSE methods in ischemic rat brain [43] and intracranial C6 tumors [15] were effective in their ability to measure ADC at diffusion times at, or below, a single millisecond, we report here the first results of these techniques in a model of tumor treatment response. Furthermore, while this study used only two gradient oscillation frequencies, with a maximum at 240 Hz, the availability of higher gradient amplitudes will allow such techniques to be pushed to higher oscillation frequencies, resulting in even shorter effective diffusion times. At such frequencies, we will be able to probe variations in tissue microstructure occurring on a submicron scale, which may provide an even more sensitive measure of the effects of chemotherapeutic agents on tumor microstructure in vivo.

Acknowledgments

We thank the National Institutes of Health, for financial support.[1]

We thank the National Institutes of Health for financial support through grants RO1CA109106, RO1NS034834, U24 CA 126588, and 1K25 EB005936. We also thank the Vanderbilt University Immunohistochemistry Core for

[1]NIH U24CA126588, 1K25 EB005936, RO1CA109106, R01NS034834, R01EB00214 and P30 CA68485

assistance in histological sectioning and staining, as well as the Vanderbilt Center for Mass Spectrometry (directed by Dr. Richard Caprioli) for assistance with digital imaging of histological data. Additionaly, we thank Mr. Jarrod True for assistance with animal care protocols.

References

1. Choyke PL, Dwyer JA, Knopp VM. Functional tumor imaging with dynamic contrast enhanced magnetic resonance imaging. J Magn Reson Imaging. 2003; 17:509–20. [PubMed: 12720260]
2. Jordan BF, Runquist M, Raghunand N, et al. Dynamic contrast-enhanced and diffusion MRI show rapid and dramatic changes in tumor microenvironment in response to inhibition of HIF-1alpha using PX-478. Neoplasia. 2005; 7:475–85. [PubMed: 15967100]
3. Padhani AR, Leach MO. Antivascular cancer treatments: functional assessments by dynamic contrast-enhanced magnetic resonance imaging. Abdom Imaging. 2005; 30:324–42. [PubMed: 15688112]
4. Yankeelov TE, Lepage M, Chakravarthy A, et al. Integration of quantitative DCE-MRI and ADC mapping to monitor treatment response in human breast cancer initial results. Magn Reson Imag. 2007; 25:1–13.
5. Sugahara T, Korogi Y, Kochi M, Ikushima I, Shigematu Y, Hirai T, Okuda T, Liang L, Ge Y, Komohara Y, Ushio Y, Takahashi M. Usefulness of diffusion-weighted MRI with echo-planar technique in the evaluation of cellularity in gliomas. J Magn Reson Imaging. 1999; 9:53–60. [PubMed: 10030650]
6. Lyng H, Haraldseth O, Rafstad EK. Measurement of cell density and necrotic fraction in human melanoma xenografts by diffusion weighted magnetic resonance imaging. Magn Reson Med. 2000; 43:828–36. [PubMed: 10861877]
7. Sinha S, Lucas-Quesada FA, Sinha U, DeBruhl N, Bassett LW. In vivo diffusion-weighted MRI of the breast: potential for lesion characterization. J Magn Reson Imaging. 2002; 15:693–704. [PubMed: 12112520]
8. Humphries PD, Sebire NJ, Siegel MJ, Olsen ØE. Tumors in pediatric patients at diffusion-weighted MR imaging: apparent diffusion coefficient and tumor cellularity. Radiology. 2007; 245:848–54. [PubMed: 17951348]
9. Zhao M, Pipe JG, Bonnett J, Evelhoch JL. Early detection of treatment response by diffusion-weighted 1H-NMR spectroscopy in a murine tumour in vivo. Br J Cancer. 1996; 73:61–4. [PubMed: 8554985]
10. Seierstad T, Folkvord S, Røe K, Flatmark K, Skretting A, Olsen DR. Early changes in apparent diffusion coefficient predict the quantitative antitumoral activity of capecitabine, oxaliplatin, and irradiation in HT29 xenografts in athymic nude mice. Neoplasia. 2007; 9:392–400. [PubMed: 17534444]
11. McConville P, Hambardzumyan D, Moody JB, Leopold WR, Kreger AR, Woolliscroft MJ, Rehemtulla A, Ross BD, Holland EC. Magnetic resonance imaging determination of tumor grade and early response to temozolomide in a genetically engineered mouse model of glioma. Clin Cancer Res. 2007; 13:2897–904. [PubMed: 17504989]
12. Morse DL, Galons JP, Payne CM, Jennings DL, Day S, Xia G, Gillies RJ. MRI-measured water mobility increases in response to chemotherapy via multiple cell-death mechanisms. NMR Biomed. 2007; 20:602–14. [PubMed: 17265424]
13. Theilmann RJ, Borders R, Trouard TP, Xia G, Outwater E, Ranger-Moore J, Gillies RJ, Stopeck A. Changes in water mobility measured by diffusion MRI predict response of metastatic breast cancer to chemotherapy. Neoplasia. 2004; 6:831–7. [PubMed: 15720810]
14. Schepkin VD, Chenevert TL, Kuszpit K, Lee KC, Meyer CR, Johnson TD, Rehemtulla A, Ross BD. Sodium and proton diffusion MRI as biomarkers for early therapeutic response in subcutaneous tumors. Magn Reson Imag. 2006; 24:273–8.
15. Colvin DC, Yankeelov TE, Does MD, Yue Z, Quarles C, Gore JC. New insights into tumor microstructure using temporal diffusion spectroscopy. Cancer Res. 2008; 68:5941–5947. [PubMed: 18632649]

16. Laws ER, Parney IF, Huang W. Survival following surgery and prognostic factors for recently diagnosed malignant glioma: data from the Gliomas Outcome Project. J Neurosurg. 2003; 99:467–73. [PubMed: 12959431]

17. Stupp R, Mason WP, van den Bent MJ, Weller M, Fisher B, Taphoorn MJ, Belanger K, Brandes AA, Marosi C, Bogdahn U, Curschmann J, Janzer RC, Ludwin SK, Gorlia T, Allgeier A, Lacombe D, Cairncross JG, Eisenhauer E, Mirimanoff RO. Radiotherapy plus concomitant and adjuvant temozolomide for glioblastoma. N Engl J Med. 2005; 352:987–96. [PubMed: 15758009]

18. Barker M, Hoshino T, Gurcay O, Wilson CB, Nielsen SL, Downie R, Eliason J. Development of an Animal Brain Tumor Model and Its Response to Therapy with 1,3-Bis(2-chloroethyl)-1-nitrosourea. Cancer Res. 1973; 33:976–86. [PubMed: 4703128]

19. Walker MD, Alexander E, Hunt WE, MacCarty CS, Mahaley MS Jr, Mealey J Jr, Norrell HA, Owens G, Ransohoff J, Wilson CB, Gehan EA, Strike TA. Evaluation of BCNU and/or radiotherapy in the treatment of anaplastic gliomas. A cooperative clinical trial. J Neurosurg. 1978; 49:333–43. [PubMed: 355604]

20. Buckner JC, Brown LD, Kugler JW, Cascino TL, Krook JE, Mailliard JA, Kardinal CG, Tschetter LK, O'Fallon JR, Scheithauer BW. Phase II evaluation of recombinant interferon alpha and BCNU in recurrent glioma. J Neurosurg. 1995; 82:430–5. [PubMed: 7861221]

21. Westphal M, Hilt DC, Bortey E, Delavault P, Olivares R, Warnke PC, Whittle IR, Jääskeläinen J, Ram Z. A phase 3 trial of local chemotherapy with biodegradable carmustine (BCNU) wafers (Gliadel wafers) in patients with primary malignant glioma. Neuro-oncol. 2003; 5:79–88. [PubMed: 12672279]

22. Fine HA, Wen PY, Maher EA, Viscosi E, Batchelor T, Lakhani N, Figg WD, Purow BW, Borkowf CB. Phase II Trial of Thalidomide and Carmustine for Patients With Recurrent High-Grade Gliomas. J Clin Oncol. 2003; 21:2299–2304. [PubMed: 12805330]

23. Feun LG, Savaraj N, Moffat F, Robinson D, Liebmann A, Hurley J, Raub WA Jr, Richman SP. Phase II trial of recombinant interferon-alpha with BCNU, cisplatin, DTIC and tamoxifen in advanced malignant melanoma. Melanoma Res. 1995; 5:273–6. [PubMed: 7496164]

24. Phillips GL, Fay JW, Herzig GP, Herzig RH, Weiner RS, Wolff SN, Lazarus HM, Karanes C, Ross WE, Kramer BS. Intensive 1,3-bis(2-chloroethyl)-1-nitrosourea (BCNU), NSC #4366650 and cryopreserved autologous marrow transplantation for refractory cancer. A phase I–II study. Cancer. 1983; 52:1792–802. [PubMed: 6354414]

25. Tchekmedyian NS, Tait N, Van Echo D, Aisner J. High-dose chemotherapy without autologous bone marrow transplantation in melanoma. J Clin Oncol. 1986; 4:1811–8. [PubMed: 3537218]

26. Elias AD, Ayash L, Frei E, Skarin AT, Hunt M, Wheeler C, Schwartz G, Mazanet R, Tepler I, Eder JP, McCauley M, Herman T, Schnipper L, Antman KH. Intensive combined modality therapy for limited-stage small-cell lung cancer. JNCI J Natl Cancer Inst. 1993; 85:559–66.

27. Turrisi AT, Sherman CA. The treatment of limited small cell lung cancer: a report of the progress made and future prospects. Eur J Cancer. 2002; 38:279–91. [PubMed: 11803144]

28. Rosenblum ML, Wheeler KT, Wilson CB, Barker M, Knebel KD. In Vitro Evaluation of in Vivo Brain Tumor Chemotherapy with 1,3-Bis(2-chloroethyl)-nitrosourea. Cancer Res. 1975; 35:1387–91. [PubMed: 1131813]

29. Rosenblum ML, Knebel KD, Vasquez DA, Wilson CB. In Vivo Clonogenic Tumor Cell Kinetics following 1,3-Bis(2-chloroethyl)-1-Nitrosourea Brain Tumor Therapy. Cancer Res. 1976; 36:2718–25.

30. Kim B, Chenevert TL, Ross BD. Growth kinetics and treatment response of the intracerebral rat 9L brain tumor model: a quantitative in vivo study using magnetic resonance imaging. Clin Cancer Res. 1995; 1:643–50. [PubMed: 9816027]

31. Ross BD, Zhao YJ, Neal ER, Stegman LD, Ercolani M, Ben-Yoseph O, Chenevert TL. Contributions of cell kill and posttreatment tumor growth rates to the repopulation of intracerebral 9L tumors after chemotherapy: an MRI study. Proc Natl Acad Sci USA. 1998; 95:7012–17. [PubMed: 9618530]

32. Neeman M, Freyer JP, Sillerud LO. A simple method for obtaining cross-term-free images for diffusion anisotropy studies in NMR microimaging. Magn Reson Med. 1991; 21:138–43. [PubMed: 1943671]

33. Rasband, WS. ImageJ. U.S. National Institutes of Health; Bethesda, Maryland, USA: 1997–2005. http://rsb.info.nih.gov/ij
34. Taxt T, Lundervold A, Fuglaas B, Lien H, Abeler V. Multispectral analysis of uterine corpus tumors in magnetic resonance imaging. Magn Reson Med. 1992; 23:55–76. [PubMed: 1734184]
35. Pham DL, Chenyang X, Prince JL. Current methods in medical image segmentation. Annu Rev Biomed Eng. 2000; 2:315–37. [PubMed: 11701515]
36. Gurcan MN, Sahiner B, Petrick N, Chan HP, Kazerooni EA, Cascade PN, Hadjiiski. Lung nodule detection on thoracic computed tomography images: Preliminary evaluation of a computer-aided diagnosis system. Med Phys. 2002; 29:2552–8. [PubMed: 12462722]
37. Stejskal EO, Tanner JE. Spin diffusion measurements: Spin echoes in the presence of a time-dependent field gradient. J Chem Phys. 1965; 42:288–92.
38. Parsons EC, Does MD, Gore JC. Modified oscillating gradient pulses for direct sampling of the diffusion spectrum suitable for imaging sequences. Magn Reson Imag. 2003; 21:279–85.
39. Arima K, Sugimura Y, Hioki T, Yamashita A, Kawamura J. Stereologically estimated mean nuclear volume of prostate cancer is a reliable prognostic parameter. Brit J Cancer. 1997; 76:234–237. [PubMed: 9231924]
40. Hsu CY, Kurman RJ, Vang R, Wang TL, Baak J, Shih Ie M. Nuclear size distinguishes low- from high-grade ovarian serous carcinoma and predicts outcome. Hum Pathol. 2005; 36:1049–1054. [PubMed: 16226103]
41. Zink D, Fischer AH, Nickerson JA. Nuclear structure in cancer cells. Nat Rev Cancer. 2004; 4:677–687. [PubMed: 15343274]
42. Xu J, Does MD, Gore JC. Sensitivity of MR diffusion measurements to variations in intracellular structure: effects of nuclear size. Magn Reson Med. 2009; 61:828–33. [PubMed: 19205020]
43. Does MD, Parsons EC, Gore JC. Oscillating gradient measurements of water diffusion in normal and globally ischemic rat brain. Magn Reson Med. 2003; 49:206–15. [PubMed: 12541239]

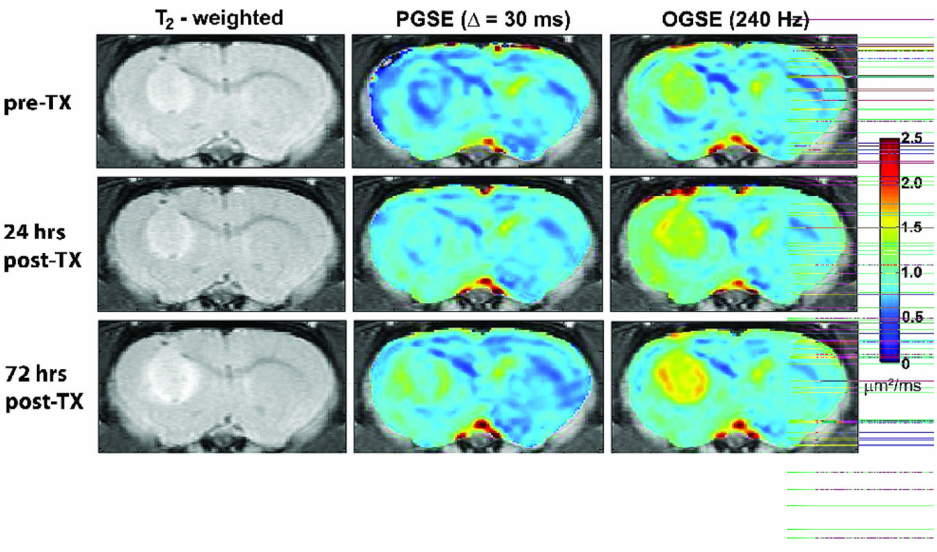

Fig. 1.

ADC maps illustrating the variation in structure of 9L tumors 24 hours and 72 hours following treatment with BCNU. The center column depicts ADC maps obtained with conventional methods, while those in the right column show results obtained with OGSE techniques (240 Hz). A corresponding color-bar representing ADC values is also shown.

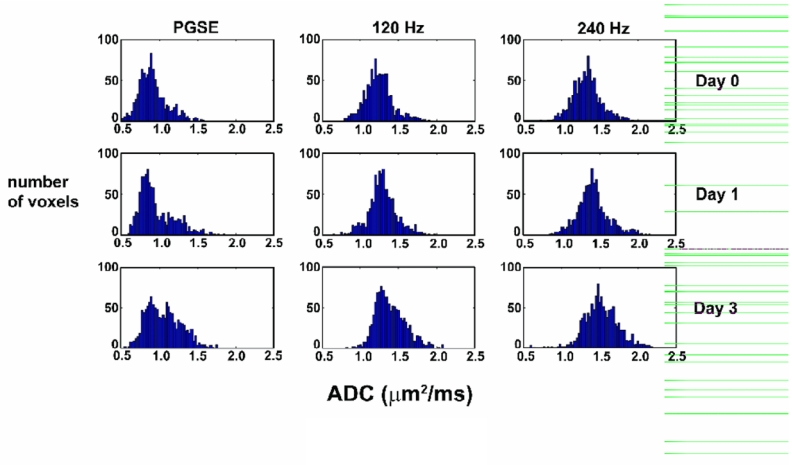

Fig. 2.

Histogram of ADC values in a whole tumor region of interest for one representative animal treated with BCNU. This figure illustrates the range of ADC values obtained within one tumor, as well as the increase in ADC following treatment. The values for PGSE are clearly lower than those obtained with OGSE techniques.

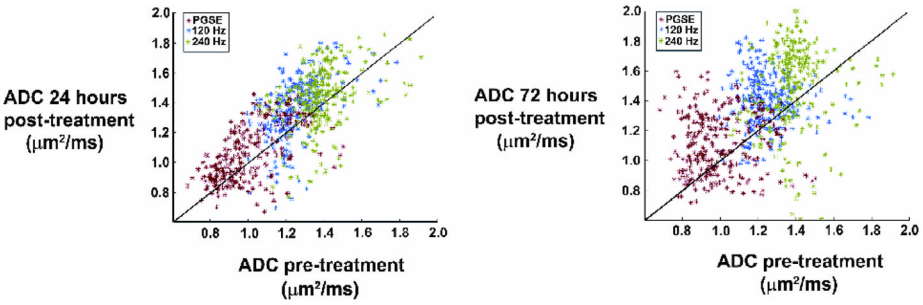

Fig. 3.

Scatter plot of ADC values for all voxels within a whole tumor region of interest 24 hours and 72 hours after treatment with BCNU. This plot illustrates an increase in ADC following treatment for all three methods, but also indicates the change in ADC for each individual voxel within the tumor.

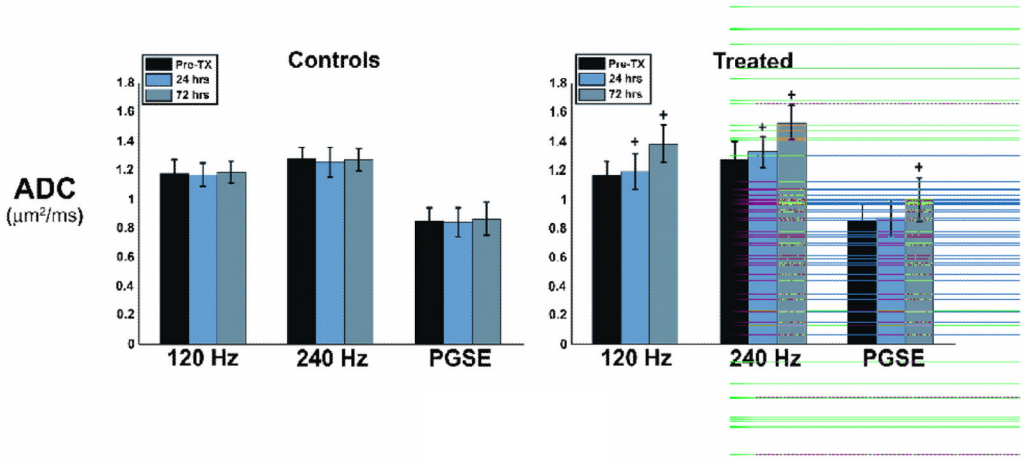

Fig. 4.

Bar graph representing the mean ADC values obtained across all animals, for both treated and control groups. Error bars represent one standard deviation of the mean. The control group shows little variation in ADC across imaging time points, while all three methods show an increase in ADC following treatment, with OGSE methods demonstrating a more pronounced effect. A '+' symbol above data bars represents a statistically significant difference in ADC from pre-treatment values at the $p < 0.05$ level.

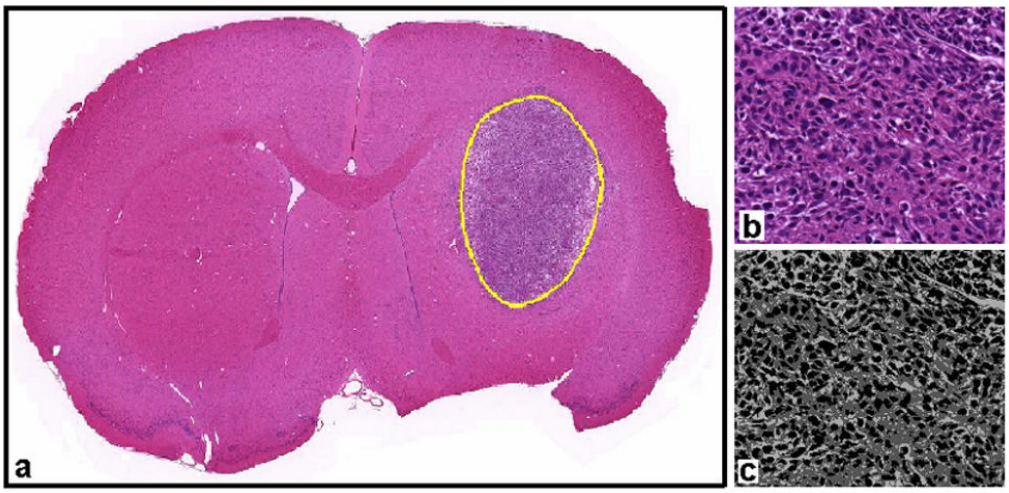

Fig. 5.

Example of histological data analysis. Whole tumor regions of interest were drawn for each sectioned tissue sample, as shown in panel (a). A close-up of one region of the tumor is shown in panel (b). A k-means clustering algorithm was used to segment H&E stained images into three regions representing the intra-nuclear, cytoplasmic, and extracellular components of the cellular space (panel (c)).

Table 1

Measurements of area fractions from histological sections

Stain	% area at 24 hours after treatment			% area at 72 hours after treatment		
	Control	Treated		Control	Treated	
Caspase-3	2.1 ± 0.7	2.4 ± 0.8	ns	2.2 ± 1.5	2.9 ± 1.4	ns
Ki-67	18.0 ± 2.4	19.8 ± 1.4	ns	19.1 ± 1.7	16.1 ± 1.6	p<.005
Extracellular space	9.2 ± 1.8	9.7 ± 1.6	ns	13.6 ± 1.8	16.2 ± 2.5	p<.05
Hemotoxylin	30.1 ± 1.2	26.9 ± 0.9	p<.002	25.9 ± 1.7	27.7 ± 1.6	p<.02
Hemotoxylin/Eosin*	42.1 ± 1.9	50.3 ± 3.7	p<.01	42.7 ± 1.9	49.5 ± 4.8	p<.008
Particle size**	37.3 ± 3.3	40.0 ± 2.5	p<.03	34.9 ± 3.6	39.3 ± 2.1	p<.05

* approximates the nuclear/intracellular fraction

** in microns^2

ns = not significant, p>0.05